

Phonon heat conduction in layered anisotropic crystals

A. J. Minnich*

Division of Engineering and Applied Science, California Institute of Technology, Pasadena, California 91125, USA

(Received 17 September 2014; revised manuscript received 9 December 2014; published 17 February 2015)

The thermal properties of anisotropic crystals are of both fundamental and practical interest, but transport phenomena in anisotropic materials such as graphite remain poorly understood because solutions of the Boltzmann equation often assume isotropy. Here, we extend an analytic solution of the transient, frequency-dependent Boltzmann equation to highly anisotropic solids and examine its predictions for graphite. We show that this simple model predicts key results, such as long c -axis phonon mean free paths and a negative correlation of cross-plane thermal conductivity with in-plane group velocity, that were previously observed with computationally expensive molecular-dynamics simulations. Further, using our analytic solution, we demonstrate a method to reconstruct the anisotropic mean free path spectrum of crystals with arbitrary dispersion relations without any prior knowledge of their harmonic or anharmonic properties using observations of quasiballistic heat conduction. These results provide a useful analytic framework to understand thermal transport in anisotropic crystals.

DOI: [10.1103/PhysRevB.91.085206](https://doi.org/10.1103/PhysRevB.91.085206)

PACS number(s): 65.40.-b

I. INTRODUCTION

Thermal transport in anisotropic crystals is of both fundamental and practical importance. Anisotropic materials can possess extreme values of thermal conductivity that are difficult to achieve in isotropic solids, with the most familiar example being graphite with an exceptional thermal conductivity of 2000 W/mK in the basal plane but only 6 W/mK in the cross-plane [1]. Graphene can be regarded as the extreme of anisotropy, and it has attracted a tremendous amount of attention [2–9]. The high in-plane thermal conductivity of graphene and graphite makes them of considerable interest for heat spreading applications [10]. At the other extreme, exceptionally low thermal conductivity has been reported in a variety of nanolaminates in the cross-plane direction [11,12], and SnTe was recently reported to possess a record high thermoelectric figure of merit due largely to the low thermal conductivity along the b axis [13]. Anisotropic materials can also exhibit a number of physical effects that do not occur in isotropic materials such as phonon focusing due to nonspherical wavefronts [14].

As a readily available and prototypical anisotropic crystal, the thermal properties of graphite have been extensively studied, starting with lattice dynamics [15–18] and thermal conductivity measurements by Slack [19], Taylor [20], and Tanaka and Suzuki [21]. Other measurements on graphite and graphite intercalation compounds were reported by Dresselhaus *et al.* [22–25]. Among the conclusions of these early works were that the phonon mean free path (MFP) along the c axis of graphite is on the order of a few nanometers at room temperature. Other anisotropic layered materials that have been recently studied experimentally include multilayered films [26], muscovite crystals [27], organoclay nanolaminates [12], and WSe₂ disordered crystals [11].

Theoretically, Klemens and Pedrazza obtained expressions for the phonon thermal conductivity of graphite assuming

a two-dimensional (2D) Debye model [28]. This treatment predicted an in-plane thermal conductivity that was in good agreement with the experimental value, but this 2D model cannot account for cross-plane heat conduction. While graphene has been studied extensively using *ab initio* calculations [5–7], most other theoretical treatments of graphite have considered only the thermal boundary conductance between graphite and other materials [29–31]. Chen *et al.* recently examined the thermal boundary conductance of anisotropic solids using an anisotropic Debye model, and they found that an isotropic model leads to a substantial overprediction of the cross-plane thermal conductance, among other inaccuracies [29]. Wei *et al.* examined the thermal conductivity of graphite using lattice dynamics and molecular dynamics (MD), concluding that a negative correlation exists between in-plane bonding strength and cross-plane thermal conductivity [32]. Heat conduction along the c axis of graphite has been studied recently using MD simulations, which indicated that the phonon MFPs are considerably longer than predicted by simple kinetic theory [33]. This prediction appears to be supported by experiment [34,35].

While these works provide important insights into thermal transport in graphite, substantially more insight into the spatial and temporal dynamics of thermal transport can be obtained using the Boltzmann transport equation (BTE) [36]. This formalism requires far less computation than MD simulations, yet it enables the dynamics of thermal transport to be calculated over a wide range of length scales, unlike formulas for thermal boundary conductance and thermal conductivity. However, the BTE is nearly always solved assuming an isotropic crystal with a spherical Brillouin zone, and thus at present many dynamic aspects of heat conduction in anisotropic crystals remain poorly understood due to the lack of a suitable theoretical approach.

Here, we investigate heat conduction in graphite using a recently reported analytic solution of the BTE [37]. This solution, which is equivalent to the Green's function of the BTE, allows an analytic description of the response of an infinite crystal to a volumetric heat input with an arbitrary temporal and 1D spatial profile. We find that just the

*aminnich@caltech.edu

incorporation of velocity anisotropy into the BTE can explain several prior results, namely long c -axis phonon MFPs and a negative correlation of cross-plane thermal conductivity with in-plane group velocity, that were obtained with expensive MD simulations. Further, we use our solution to develop a reconstruction method that allows the anisotropic MFP spectrum to be obtained from observations of quasiballistic transport without any prior knowledge of the harmonic or anharmonic properties of the crystal. Our work provides an analytic framework to understand the dynamics of thermal transport in anisotropic crystals.

The paper is organized as follows. First, in Sec. II we derive the general solution to the BTE assuming an infinite crystal is subject to volumetric heat generation with an arbitrary temporal and 1D spatial profile. We then derive simplifications of this solution to enable analytic insights and specialize the equations to graphite. In Sec. III, we examine the effect of velocity anisotropy on the thermal conductivity and the transient response of the anisotropic crystal to heat impulses oriented along different crystallographic directions. Finally, we use these results to develop a method that can reconstruct the MFP spectrum of a crystal with an arbitrary dispersion relation.

II. THEORY

A. General solution of the BTE

We begin by briefly reviewing the derivation of the transport solution to the BTE as presented by Hua and Minnich for an isotropic crystal [37] and generalized to a solid with an arbitrary dispersion relation by Vermeersch *et al.* [38]. The one-dimensional BTE under the relaxation-time approximation for transport along the z direction is given by

$$\frac{\partial g_{\mathbf{k}}}{\partial t} + v_{z\mathbf{k}} \frac{\partial g_{\mathbf{k}}}{\partial z} = -\frac{g_{\mathbf{k}} - g_0(T(z,t))}{\tau_{\mathbf{k}}} + Q_{\mathbf{k}}, \quad (1)$$

where $g_{\mathbf{k}} = \hbar\omega[f_{\mathbf{k}}(z,t) - f_0(T_0)]$ is the desired deviational distribution function, $Q_{\mathbf{k}}(z,t)$ is the spectral volumetric heat generation, $v_{z\mathbf{k}}$ is the component of the phonon group velocity along the z direction, $\tau_{\mathbf{k}}$ is the phonon relaxation time, and \mathbf{k} is the phonon wave vector in phase space. $g_0(T(z,t))$ is the local equilibrium deviational distribution function and is given by

$$g_0(T(z,t)) = \hbar\omega[f_{\text{BE}}(T(z,t)) - f_0(T_0)] \approx C_{\mathbf{k}}\Delta T(z,t), \quad (2)$$

assuming a small temperature rise $\Delta T(z,t) = T(z,t) - T_0$ relative to a reference temperature T_0 . Here, \hbar is the reduced Planck constant, $\omega(\mathbf{k})$ is the phonon frequency given by the dispersion relation, $f_{\text{BE}}(T(z,t))$ is the local Bose-Einstein distribution, $f_0(T_0)$ is the Bose-Einstein distribution at T_0 , and $C_{\mathbf{k}} = N_{\text{pol}}k_B[\chi/\sinh(\chi)]^2$ is the mode-specific heat, where $\chi = \hbar\omega/2k_B T_0$ and N_{pol} is the number of polarizations. To close the problem, energy conservation is used to relate $g_{\mathbf{k}}$ to $\Delta T(z,t)$ as

$$\sum_{\mathbf{k}} \left[\frac{g_{\mathbf{k}}}{\tau_{\mathbf{k}}} - \frac{C_{\mathbf{k}}}{\tau_{\mathbf{k}}} \Delta T(z,t) \right] = 0, \quad (3)$$

where the sum is performed over all phonon modes in the Brillouin zone.

An analytic solution to the above equations is obtained by performing a Fourier transform over z and t in Eq. (1),

substituting the result into Eq. (3), and solving for the temperature response $\Delta\tilde{T}(\eta, \xi_z)$, where η and ξ_z are the Fourier variables in the time and spatial domains, respectively [37]. This procedure assumes that the thermal transport occurs in an infinite domain so that a Fourier transform can be performed. The result is

$$\Delta\tilde{T}(\eta, \xi_z) = \frac{\sum_{\mathbf{k}} \tilde{Q}_{\mathbf{k}} \gamma_{\mathbf{k}}^{-1}}{\sum_{\mathbf{k}} C_{\mathbf{k}} \tau_{\mathbf{k}}^{-1} (1 - \gamma_{\mathbf{k}}^{-1})}, \quad (4)$$

where $\gamma_{\mathbf{k}} = 1 + i\eta\tau_{\mathbf{k}} + i\xi_z\Lambda_{z\mathbf{k}}$ and $\Lambda_{z\mathbf{k}} = v_{z\mathbf{k}}\tau_{\mathbf{k}}$ is the component of the MFP along the z direction. Once $\Delta\tilde{T}$ is determined, $\tilde{g}_{\mathbf{k}}$ can be expressed as

$$\tilde{g}_{\mathbf{k}} = (C_{\mathbf{k}}\Delta\tilde{T} + \tilde{Q}_{\mathbf{k}}\tau_{\mathbf{k}})\gamma_{\mathbf{k}}^{-1}. \quad (5)$$

The heat flux \tilde{q}_z along the z direction is given by

$$\tilde{q}_z = \frac{1}{V} \sum_{\mathbf{k}} \tilde{g}_{\mathbf{k}} v_{z\mathbf{k}}, \quad (6)$$

where V is the volume of the crystal. Solutions to each of these quantities in real space can be easily obtained by an inverse Fourier transform. This solution is valid for a crystal with an arbitrary dispersion relation. In the diffusive limit, these equations reduce to Fourier's law with a thermal conductivity given by

$$\kappa_z = \frac{1}{V} \sum_{\mathbf{k}} C_{\mathbf{k}} v_{z\mathbf{k}}^2 \tau_{\mathbf{k}}. \quad (7)$$

B. Weak quasiballistic regime

We now derive a simplified solution to these equations under the assumption that $\eta\tau \ll 1$. This regime, previously denoted the weak quasiballistic regime by Hua and Minnich [37], physically indicates that length scales are comparable to MFPs but the relevant time scales are much longer than relaxation times. This situation frequently occurs in thermal experiments such as transient grating spectroscopy for which grating periods $\lambda = 2\pi/\xi_z$ are on a micron length scale but thermal decay times are tens to hundreds of nanoseconds, far longer than typical relaxation times [39].

The term $\gamma_{\mathbf{k}}^{-1}$ can be written as

$$\gamma_{\mathbf{k}}^{-1} = \frac{1}{1 + i\eta\tau_{\mathbf{k}} + ix} = \sum_{n=0}^{\infty} (-1)^n (i\eta\tau_{\mathbf{k}} + ix)^n. \quad (8)$$

Expanding the polynomial and neglecting higher-order terms in $\eta\tau_{\mathbf{k}}$ yields

$$\gamma_{\mathbf{k}}^{-1} = \sum_{n=0}^{\infty} (-ix)^n [1 - i(n+1)\eta\tau_{\mathbf{k}}]. \quad (9)$$

These sums can be performed using the standard geometric series formula as

$$1 - \gamma_{\mathbf{k}}^{-1} = \frac{i\eta\tau_{\mathbf{k}}}{(1+ix)^2} + 1 - \frac{1}{1+ix}. \quad (10)$$

Substituting this result into the denominator of Eq. (4) gives

$$\sum_{\mathbf{k}} \frac{C_{\mathbf{k}}}{\tau_{\mathbf{k}}} (1 - \gamma_{\mathbf{k}}^{-1}) = \sum_{\mathbf{k}} \frac{i\eta C_{\mathbf{k}}}{(1 + ix)^2} + \frac{q^2}{V} \sum_{\mathbf{k}} C_{\mathbf{k}} v_{z\mathbf{k}}^2 \tau_{\mathbf{k}} \left[\frac{1}{x^2} \left(1 - \frac{1}{1 + ix} \right) \right]. \quad (11)$$

Inserting this result into Eq. (4) and simplifying yields ΔT under the assumption $\eta\tau \ll 1$:

$$\Delta T = \frac{Q}{i\eta C + q^2 V^{-1} \sum_{\mathbf{k}} \kappa_{z\mathbf{k}} (1 + x^2)^{-1}}, \quad (12)$$

where the spectral thermal conductivity $\kappa_{z\mathbf{k}} = C_{\mathbf{k}} v_{z\mathbf{k}}^2 \tau_{\mathbf{k}}$. To obtain this result, we have neglected quasiballistic terms multiplying $i\eta C$ as in the weakly quasiballistic regime ballistic modes have a small contribution to the heat capacity. We also assume that $Q_{\mathbf{k}} \sim C_{\mathbf{k}}$, allowing us to use the same assumption to simplify the numerator. Finally, we have retained only the real part of Eq. (11) as the imaginary part is odd and sums to zero.

Comparing this result with the Green's function of the heat equation, $\Delta T(\xi_z, \eta) = Q \times (i\eta C + q^2 \kappa_z)^{-1}$, we observe that in the weakly quasiballistic regime, the effective thermal conductivity can be expressed as

$$\kappa_{\text{eff}} = \frac{1}{V} \sum_{\mathbf{k}} \kappa_{z\mathbf{k}} S(x), \quad (13)$$

where $S(x) = (1 + x^2)^{-1}$ is the suppression function. This result is identical to that derived previously by Hua and Minnich [37] with two important differences. First, this result is valid for a crystal with an arbitrary dispersion relation, unlike the prior result, which is valid only for isotropic crystals. Second, the independent variable $x = \xi_z \Lambda_{z\mathbf{k}}$ contains the component of the MFP along the transport direction rather than the magnitude of the MFP as in the isotropic case.

C. Application to graphite

We now seek to use this solution to study thermal transport in highly anisotropic materials. In this work, we focus on graphitelike layered crystals with a dispersion given by an anisotropic Debye model [27,29]. While the Debye model has known shortcomings for transport calculations [40], in particular the neglect of the acoustic branch with a quadratic dispersion, for the present work it is sufficient to describe the key physics while enabling analytic expressions for transport quantities. As will be shown in Sec. III, the anisotropy of thermal conductivity is largely driven by the mismatch in phonon frequencies along each crystallographic direction rather than the specific dispersion relation, and thus the specific choice of dispersion relation does not affect our conclusions.

In the anisotropic Debye model, the dispersion relation is given by

$$\omega^2 = v_{ab}^2 k_{ab}^2 + v_c^2 k_c^2, \quad (14)$$

where v_{ab} and k_{ab} are the sound velocity and wave vector along the ab direction, and v_c and k_c are the corresponding quantities for the c direction. This form of the dispersion

assumes that symmetry exists in two of the crystal directions such that $v_a = v_b = v_{ab}$. We take the ab direction to represent the in-plane direction of graphite while c represents the cross-plane direction. The phonon group velocity along the crystal axis j is given as

$$v_j = \frac{\partial \omega}{\partial k_j} = \frac{v_{j,s}^2 k_j}{\omega(\mathbf{k})}, \quad (15)$$

where $v_{j,s}$ is the sound velocity.

The transport properties for a solid with this dispersion can be expressed as sums, as presented in Sec. II, over the phase-space states contained in an ellipsoidal Brillouin zone specified by

$$\frac{k_{ab}^2}{k_{ab,m}^2} + \frac{k_c^2}{k_{c,m}^2} = \hat{k}_{ab}^2 + \hat{k}_c^2 = 1, \quad (16)$$

where $k_{j,m}$ denote the maximum wave vectors in the Brillouin zone along crystal axis j , and \hat{k}_j are wave vectors normalized to $k_{j,m}$. The sums over phase space in Sec. II B can be simplified by replacing them with integrals over the ellipsoidal Brillouin zone using the relation $V^{-1} \sum_{\mathbf{k}} = (2\pi)^{-3} \int d^3\mathbf{k}$. This integral can then be further simplified by transforming the volume of integration to a unit sphere. To do so, we define $k_c = \hat{k}_{c,m} \cos \theta$, $k_a = \hat{k}_{ab,m} \sin \theta \cos \phi$, and $k_b = \hat{k}_{ab,m} \sin \theta \sin \phi$, and $\hat{k}^2 = \hat{k}_{ab}^2 + \hat{k}_c^2$. The resulting relation between the sum and the integral is then:

$$\frac{1}{V} \sum_{\mathbf{k}} b(\mathbf{k}) = A \int_0^{2\pi} \int_{-1}^1 \int_0^1 b(\hat{k}, \mu, \phi) \hat{k}^2 d\hat{k} d\mu d\phi, \quad (17)$$

where b is an arbitrary function of \mathbf{k} , $\mu = \cos \theta$, and $A = k_{c,m} k_{ab,m}^2 / (2\pi)^3$.

Using this transformation, the temperature response $\Delta \tilde{T}_j$ for heat input $\tilde{Q}_{\mathbf{k}}(\eta, \xi_z)$ when the z axis is aligned with crystal axis j is

$$\Delta \tilde{T}_j(\eta, \xi_z) = \frac{\int_0^1 \int_{-1}^1 \tilde{Q}_{\mathbf{k}} G_j \hat{k}^2 d\hat{k} d\mu}{\int_0^1 \int_{-1}^1 C_{\mathbf{k}} \tau_{\mathbf{k}}^{-1} [1 - G_j] \hat{k}^2 d\hat{k} d\mu}, \quad (18)$$

where $G_c = 2\pi \gamma_{\mathbf{k}}^{-1}$ with $v_{z\mathbf{k}} = v_{c\mathbf{k}}$, and G_{ab} is given by

$$G_{ab} = \frac{2\pi}{\sqrt{(1 + i\eta\tau_{\mathbf{k}})^2 + x_{ab}^2}}. \quad (19)$$

Equation (19) was obtained through the use of identity 3.661.3 in Ref. [41] to perform the integral over ϕ .

The heat flux \tilde{q}_j is given by

$$q_j = A \int_{-1}^1 \int_0^1 g_{\mathbf{k}} v_{j\mathbf{k}} H_j \hat{k}^2 d\hat{k} d\mu, \quad (20)$$

where $H_c = 2\pi \gamma_{\mathbf{k}}^{-1}$ and

$$H_{ab} = \frac{2\pi}{ix_{ab}} \left(1 - \sqrt{\frac{(1 + i\eta\tau_{\mathbf{k}})^2}{(1 + i\eta\tau_{\mathbf{k}})^2 + x_{ab}^2}} \right). \quad (21)$$

This result was obtained using the following identity:

$$\int_0^{2\pi} \frac{\cos \phi}{a + b \cos \phi} d\phi = \frac{2\pi}{b} \left(1 - \sqrt{\frac{a^2}{a^2 - b^2}} \right). \quad (22)$$

The thermal conductivity κ_j can be written

$$\kappa_j = A_j \int_{-1}^1 \int_0^1 C_{\mathbf{k}} v_{j,\mathbf{k}}^2 \tau_{\mathbf{k}} \hat{k}^2 d\hat{k} d\mu = A_j \int_{-1}^1 \int_0^1 \kappa_{j\mathbf{k}} \hat{k}^2 d\hat{k} d\mu, \quad (23)$$

where $A_c = 2\pi A$ and $A_{ab} = \pi A$. Finally, the effective thermal conductivity in the weakly quasiballistic regime presented in Sec. II B is given by

$$\kappa_{\text{eff},j} = 2\pi A \int_{-1}^1 \int_0^1 \kappa_{j\mathbf{k}} S_j \hat{k}^2 d\hat{k} d\mu, \quad (24)$$

where $S_c = (1 + x_c^{-2})^{-1}$ and

$$S_{ab} = \frac{1}{x_{ab}^2} \left(1 - \frac{1}{\sqrt{1 + x_{ab}^2}} \right), \quad (25)$$

where $x_j = \xi_z \Lambda_{j\mathbf{k}}$. This result was obtained using the relation

$$\int_0^{2\pi} \frac{\cos^2 \phi}{a + b \cos^2 \phi} d\phi = \frac{2\pi}{b} \left(1 - \sqrt{\frac{a}{a+b}} \right). \quad (26)$$

To model graphite, we take the sound velocities to be $v_{ab} = 15$ km/s and $v_c = 1$ km/s. The relationship between the number density and the maximum wave vectors to ensure the correct number of modes is [29]

$$n_{\text{puc}} = \frac{1}{6\pi^2} (k_{c,m} k_{ab,m}^2)^{1/3}. \quad (27)$$

We consider only acoustic phonons, and thus $n_{\text{puc}} = n/4$ represents the number density of primitive unit cells, where $n = 1.13 \times 10^{29} \text{ m}^{-3}$ is the atomic number density in graphite. Incorporating the anisotropy of the actual lattice constant of graphite, we obtain $k_{ab,m} = 13.0 \text{ nm}^{-1}$ and $k_{c,m} = 9.7 \text{ nm}^{-1}$. These maximum wave vectors correspond to lattice constants of $a_{ab} = 2.38 \text{ \AA}$ and $a_c = 3.32 \text{ \AA}$, quite close to the actual lattice constants of $a_{ab} = 2.46 \text{ \AA}$ and $a_c = 3.35 \text{ \AA}$, respectively. The relaxation times are chosen to be

$$\tau^{-1} = \frac{10^{17}}{\omega(\mathbf{k})^2} + \frac{v}{L_b}, \quad (28)$$

where $L_b = 1$ mm is a boundary scattering length scale and v is the velocity of a particular mode. We assume that three identical polarizations exist. These parameters yield $\kappa_{ab} = 2680$ W/mK and $\kappa_c = 4$ W/mK, reasonably close to the literature values of 2000 and 6 W/mK, respectively [1].

We have made two assumptions in the relaxation-time model. First, we assume the relaxation time to be isotropic, as the actual phonon relaxation times and their anisotropy in graphite are unknown. However, the relaxation times appear to be isotropic to first order because the calculated thermal conductivity is in reasonable agreement with experiment, thus supporting our treatment.

Second, we have assumed the relaxation times to scale as ω^{-2} , although first-principles calculations suggest that this scaling could vary as ω^{-1} for some low-frequency phonons [42]. We have verified that assuming a different scaling of the relaxation time with frequency does not affect our conclusions, and so we proceed with the form specified above.

III. RESULTS

A. Thermal conductivity

We first investigate the correlation between the thermal conductivity along the c - and ab -axes by calculating the thermal conductivities as a function of c - and ab -axis group velocity. A prior work used MD simulations to conclude that a negative correlation exists between cross-plane thermal conductivity and in-plane bonding strength, which is directly related to the group velocity [32].

Figures 1(a) and 1(b) plot the ab - and c -axis thermal conductivities as a function of the c -axis or ab -axis group velocity, respectively. This plot shows the expected result that decreasing the group velocity also decreases the thermal conductivity along that direction. However, the plot also reveals the negative correlation: the thermal conductivity along a particular crystal axis increases as the group velocity decreases in the perpendicular crystal axis. For example, in Fig. 1(b), decreasing the ab -axis velocity increases the c -axis thermal conductivity.

The reason for this trend has been described in detail by Wei *et al.* [32] and is due to the highly elliptical isofrequency surface. The group velocity along a particular crystallographic direction equals the component of the gradient of the isofrequency surface along that direction. As the fast direction group velocity decreases, the Brillouin zone becomes more spherical and increases the average group velocity along the slow direction, leading to a higher thermal conductivity along the slow direction even while the thermal conductivity decreases in the fast direction. While Ref. [32] used MD simulations with variable bonding strengths to identify this negative correlation, our calculation shows that the same trend can be observed simply by incorporating anisotropic group velocities into the BTE. Our result thus provides an analytical framework to understand anisotropic effects much more easily than with numerical MD simulations.

We point out another counterintuitive result in the isotropic limit: the thermal conductivity when the group velocity along all three directions is 1 km/s, Fig. 1(b), is slightly larger than that when all group velocities equal 15 km/s, Fig. 1(a), though from the kinetic equation the opposite trend is expected. The discrepancy can be explained by differences in the phonon frequency spectrum in each direction. In the case in which the group velocity is 1 km/s, the maximum frequency is around 2 THz and all modes are occupied since $k_B T/h \approx 6$ THz at $T = 300$ K. In the latter case, the maximum phonon frequency is around 31 THz and many modes remain unoccupied, resulting in a smaller specific heat and slightly smaller thermal conductivity than in the former case. Thus when considering the origin of thermal conductivity anisotropy, it is important to compare the occupation of modes along different directions. The difference in occupation is particularly large for graphite because many of the stiff, high-frequency in-plane modes remain unoccupied at room temperature, while essentially all of the soft, low-frequency cross-plane modes are occupied.

Also, note from Fig. 1(b) that the thermal conductivity when all group velocities equal 1 km/s is orders of magnitude larger than the c -axis value of graphite. This observation highlights that a primary reason that the c -axis thermal conductivity is low is actually because the ab -axis group velocity is high.

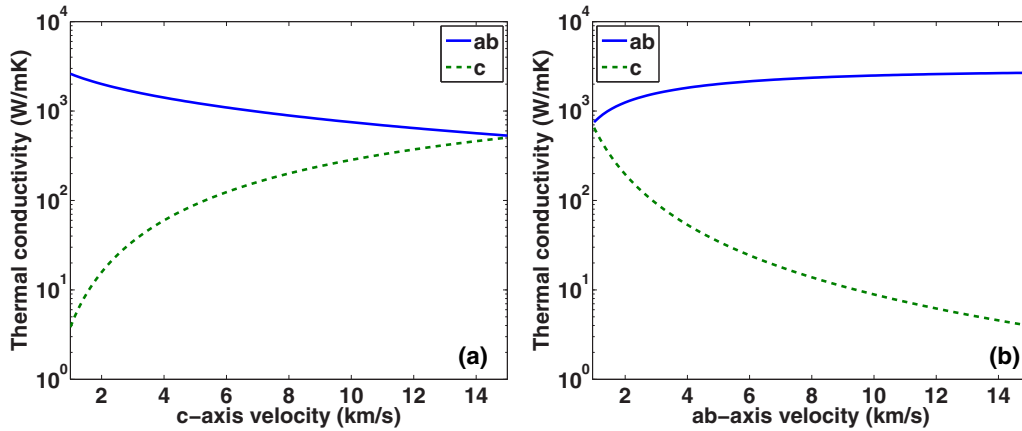


FIG. 1. (Color online) Thermal conductivity of graphite along the ab axis and the c axis as (a) the c -axis velocity is varied and the ab -axis velocity is fixed at 15 km/s, and (b) the ab -axis velocity is varied and the c -axis velocity is fixed at 1 km/s. Decreasing the c -axis velocity increases the ab -axis thermal conductivity, while decreasing the ab -axis velocity increases the c axis thermal conductivity.

The difference in group velocities leads to a highly elliptical isofrequency surface that decreases the group velocity along the c axis as discussed above and in Ref. [32].

B. Transient thermal response

We now use our solution to investigate the dynamics of thermal transport in the quasiballistic regime in which thermal gradients occur over length scales comparable to MFPs. For the rest of the paper, we consider graphite with $v_{ab} = 15$ km/s and $v_c = 1$ km/s. First, we calculate the transient temperature response assuming the heating profile is a spatially sinusoidal impulse with period $\lambda = 2\pi/\xi_x$ as occurs in transient grating experiments [39]. The thermal decay is obtained by performing an inverse fast Fourier transform on Eq. (18) and is shown in Fig. 2. For a grating period of 1 mm along the ab axis, the heat conduction is diffusive and the BTE solution agrees with Fourier's law, as in Fig. 2(a). For a grating period of 20 μm , Fig. 2(b), the thermal decay deviates from the Fourier law prediction, indicating that MFPs are comparable to the grating period. Such long MFPs could be expected given the large thermal conductivity along the ab axis. The thermal decay from the BTE is in excellent agreement with a modified Fourier law with a thermal conductivity given by Eq. (13), as expected based on the derivation in Sec. II B.

The corresponding results for the c axis are presented in Figs. 2(c) and 2(d). Similarly to the ab axis, the heat conduction is diffusive for a grating period of 1 mm. For a grating period of 20 μm , however, significant quasiballistic effects are observed in Fig. 2(d). This observation is initially unexpected because the c -axis thermal conductivity is 250 times smaller than the ab -axis value, yet the c -axis MFPs appear to be comparable to those along the ab -axis.

The presence of phonons with long c axis MFPs was previously observed using MD simulations and was attributed to the fact that high-frequency phonons are not supported along the c axis [33]. Any estimation of an average MFP using kinetic theory and the bulk specific heat will therefore dramatically underestimate the MFP. Another explanation for the long c axis MFPs using our BTE solution can be found in the relaxation times. Recall that we have assumed the

relaxation times to depend only on the phonon frequency. Since only low-frequency phonons are supported along the c axis, these phonons have long relaxation times and hence long MFPs. The c -axis MFPs are thus only smaller than those along the ab axis by a factor on the order of the velocity anisotropy ratio, equal to 15 for graphite. However, these long MFPs contribute substantially to c -axis thermal conductivity as higher-frequency phonons with shorter MFPs are not supported along the c axis. In this way, the c -axis thermal conductivity can be small even though the phonons carrying the heat can have long MFPs. While long c -axis MFP phonons were originally identified using MD simulations, our BTE approach is much more tractable for studying transport properties in anisotropic crystals because all quantities can be represented analytically.

C. MFP spectrum reconstruction

We now arrive at the principal topic of our study. MFP spectroscopy has emerged as a useful technique to recover the MFP spectrum of crystals solely from transient thermal decays such as those presented in Fig. 2 [43]. However, analysis of the data using the BTE has typically assumed the crystal to be isotropic and thus it cannot be applied to arbitrary crystals [44]. It would be highly desirable to generalize this technique so that the MFP spectrum of an anisotropic crystal can be extracted from the transient thermal decays without requiring any prior knowledge of the harmonic properties or anisotropy of the lattice.

This procedure is in fact possible using the analytic solution we have derived in Sec. II B. To see how to recover the anisotropic MFP spectrum, consider Eq. (13), which expresses the effective thermal conductivity κ_{eff} as a function of the spectral thermal conductivity $\kappa_{z\mathbf{k}}$ and a suppression function $S(x)$, where $x = \xi_z \Lambda_{z\mathbf{k}}$. This equation has exactly the same form as that presented in Ref. [44] with the exception that the MFP is no longer the isotropic MFP Λ but rather the component of the MFP along the transport direction $\Lambda_{z\mathbf{k}}$. This observation suggests that a generalized reconstruction approach can be implemented to obtain the MFP spectrum of a crystal with an arbitrary dispersion relation by letting

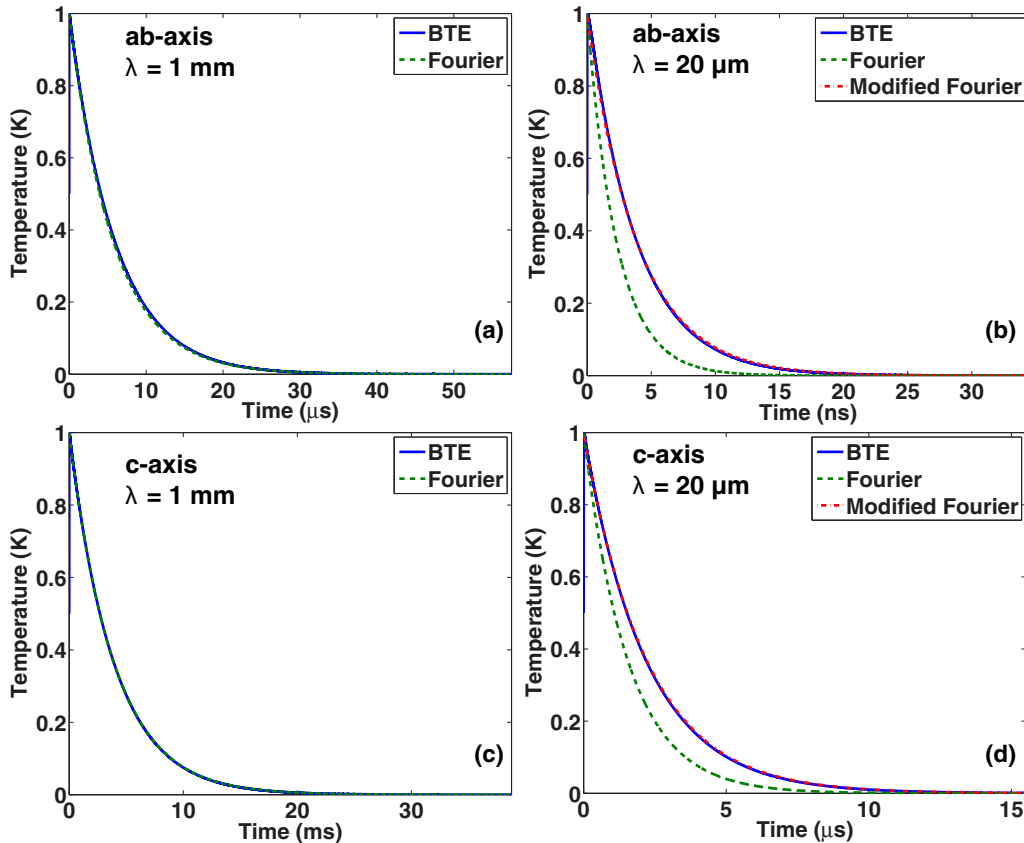


FIG. 2. (Color online) Temperature decay vs time for a spatially sinusoidal heat impulse with grating period λ for (a) the ab axis and $\lambda = 1$ mm; (b) the ab axis and $\lambda = 20 \mu\text{m}$; (c) the c axis and $\lambda = 1$ mm; and (d) the c axis and $\lambda = 20 \mu\text{m}$. In the diffusive limit, (a) and (c), the BTE solution agrees with diffusion theory. In the quasiballistic limit, (b) and (d), the BTE solution agrees with a modified Fourier law with a thermal conductivity given by Eq. (13). Note that quasiballistic effects are apparent along both the ab and c axes even though the thermal conductivity is much smaller along the c axis.

the independent variable be $\Lambda_{z\mathbf{k}}$ rather than Λ . The sum over phase space can then be transformed into an integral over $\Lambda_{z\mathbf{k}}$, yielding an equation exactly analogous to that considered by Chen and Dames [29] and Minnich [44]. Then, the anisotropic MFP spectrum can be obtained from the effective thermal conductivities using the method of Ref. [44] without any knowledge of the anisotropy, harmonic properties, or the MFPs of the material of interest.

We demonstrate this approach using the numerical method exactly as described in Ref. [44]. Briefly, we synthesize effective thermal conductivities numerically using Eq. (13) and add artificial random noise to simulate experimental uncertainty. Using these effective thermal conductivities and our knowledge of the suppression function, we use CVX [45,46] to solve for the generalized MFP spectrum. The result is shown in Fig. 3, demonstrating excellent agreement between the reconstructed and actual MFP spectra along both the ab and c axes. This result shows that our approach can accurately reconstruct the anisotropic MFP spectrum along different crystallographic directions with only the effective thermal conductivities and the known suppression function as input.

As predicted previously by MD simulations [33], Fig. 3 demonstrates that the MFPs responsible for heat conduction

along the ab and c axes can be comparable even though the calculated thermal conductivities differ by a factor of over 600. This result indicates that in anisotropic crystals, scattering is not the sole origin of low thermal conductivity as is typically assumed for isotropic crystals. Instead, low thermal conductivity can originate from the group velocity and phonon frequencies that are supported along each crystallographic direction as determined by the shape of the isofrequency surface. Clearly, properly incorporating a realistic shape of the isofrequency surface is essential to making accurate predictions of thermal transport in anisotropic crystals. Our work demonstrates that the BTE can be used to study thermal transport in anisotropic crystals with an arbitrary dispersion relation at minimal computational cost compared to MD simulations while predicting the key features of the transport phenomena.

Finally, we note that the MFPs in actual graphite are unlikely to be as long as those presented in Fig. 3. MD simulations report the c -axis MFPs to be on the order of a few hundred nanometers [33]. The predictions in the present work could likely be improved by incorporating the exact dispersion for graphite from lattice dynamics, an effort that we will address in a future work.

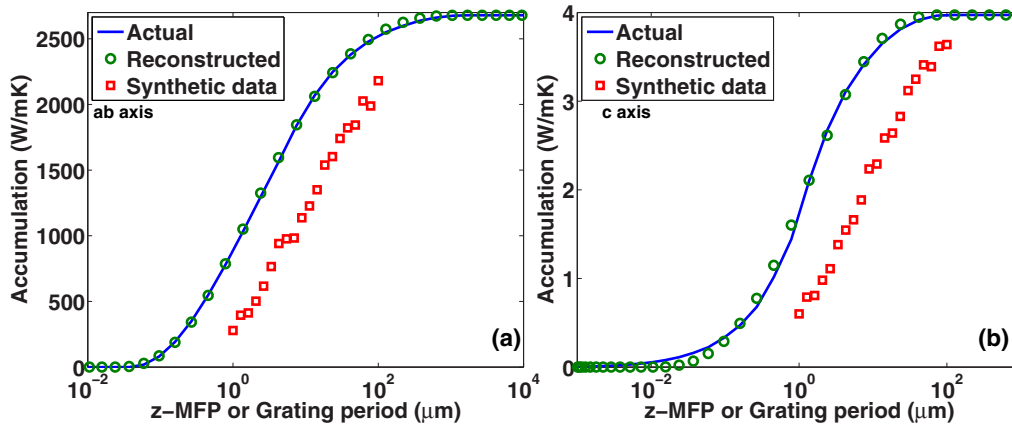


FIG. 3. (Color online) Accumulated MFP spectrum vs component of MFP along the transport direction (z -MFP) or grating period (for synthetic data) along (a) the ab axis and (b) the c axis. The synthesized thermal conductivities with added random noise are the red squares, the actual MFP spectrum is the blue line, and the result of the reconstruction is the green circles. Our reconstruction approach can determine the generalized MFP spectrum without any knowledge of the harmonic or anharmonic properties of the crystal.

IV. SUMMARY

We have used an analytic solution of the BTE to study heat conduction in graphite. We show that our simple analytic framework can predict key features of the transport phenomena reported earlier using MD simulations. Further, we have used our analytic BTE solution to develop a generalized MFP spectrum reconstruction method that enables the anisotropic MFP spectrum to be reconstructed without any prior knowledge of the properties of the crystal. Our result provides a better understanding of heat conduction in anisotropic crystals and the theoretical basis necessary to

directly measure the phonon MFP spectrum in a wide range of crystals.

ACKNOWLEDGMENTS

The author thanks Chengyun Hua and Ding Ding for performing several integrals. This work was sponsored in part by Robert Bosch LLC through Bosch Energy Research Network Grant No. 13.01.CC11, by the National Science Foundation under Grant No. CBET CAREER 1254213, and by Boeing under the Boeing-Caltech Strategic Research & Development Relationship Agreement.

- [1] Y. S. Touloukian, *Thermophysical Properties of Matter: Thermal Conductivity: Nonmetallic Solids* (IFI/Plenum, New York, 1970).
- [2] W. Jang, Z. Chen, W. Bao, C. N. Lau, and C. Dames, Thickness-dependent thermal conductivity of encased graphene and ultrathin graphite, *Nano Lett.* **10**, 3909 (2010).
- [3] S. Ghosh, W. Bao, D. L. Nika, S. Subrina, E. P. Pokatilov, C. N. Lau, and A. A. Balandin, Dimensional crossover of thermal transport in few-layer graphene, *Nat. Mater.* **9**, 555 (2010).
- [4] J. H. Seol, I. Jo, A. L. Moore, L. Lindsay, Z. H. Aitken, M. T. Pettes, X. Li, Z. Yao, R. Huang, D. Broido *et al.*, Two-dimensional phonon transport in supported graphene, *Science* **328**, 213 (2010).
- [5] N. Bonini, J. Garg, and N. Marzari, Acoustic phonon lifetimes and thermal transport in free-standing and strained graphene, *Nano Lett.* **12**, 2673 (2012).
- [6] L. Lindsay, W. Li, J. Carrete, N. Mingo, D. A. Broido, and T. L. Reinecke, Phonon thermal transport in strained and unstrained graphene from first principles, *Phys. Rev. B* **89**, 155426 (2014).
- [7] L. Paulatto, F. Mauri, and M. Lazzeri, Anharmonic properties from a generalized third-order *ab initio* approach: Theory and applications to graphite and graphene, *Phys. Rev. B* **87**, 214303 (2013).
- [8] M.-H. Bae, Z. Li, Z. Aksamija, P. N. Martin, F. Xiong, Z.-Y. Ong, I. Knezevic, and E. Pop, Ballistic to diffusive crossover of heat flow in graphene ribbons, *Nat. Commun.* **4**, 1734 (2013).
- [9] X. Xu, L. F. C. Pereira, Y. Wang, J. Wu, K. Zhang, X. Zhao, S. Bae, C. Tinh Bui, R. Xie, J. T. L. Thong *et al.*, Length-dependent thermal conductivity in suspended single-layer graphene, *Nat. Commun.* **5**, 3689 (2014).
- [10] Z. Yan, G. Liu, J. M. Khan, and A. A. Balandin, Graphene quilts for thermal management of high-power GaN transistors, *Nat. Commun.* **3**, 827 (2012).
- [11] C. Chiritescu, D. G. Cahill, N. Nguyen, D. Johnson, A. Bodapati, P. Keblinski, and P. Zschack, Ultralow thermal conductivity in disordered, layered WSe₂ crystals, *Science* **315**, 351 (2007).
- [12] M. D. Losego, I. P. Blitz, R. A. Vaia, D. G. Cahill, and P. V. Braun, Ultralow thermal conductivity in organoclay nanolaminates synthesized via simple self-assembly, *Nano Lett.* **13**, 2215 (2013).
- [13] L.-D. Zhao, S.-H. Lo, Y. Zhang, H. Sun, G. Tan, C. Uher, C. Wolverton, V. P. Dravid, and M. G. Kanatzidis, Ultralow thermal conductivity and high thermoelectric figure of merit in SnSe crystals, *Nature (London)* **508**, 373 (2014).

- [14] R. J. von Gutfeld and A. H. Nethercot, Heat pulses in quartz and sapphire at low temperatures, *Phys. Rev. Lett.* **12**, 641 (1964).
- [15] R. Al-Jishi and G. Dresselhaus, Lattice-dynamical model for graphite, *Phys. Rev. B* **26**, 4514 (1982).
- [16] R. Nicklow, N. Wakabayashi, and H. G. Smith, Lattice dynamics of pyrolytic graphite, *Phys. Rev. B* **5**, 4951 (1972).
- [17] J. C. Bowman and J. A. Krumhansl, The low-temperature specific heat of graphite, *J. Phys. Chem. Solids* **6**, 367 (1958).
- [18] J. Krumhansl and H. Brooks, The lattice vibration specific heat of graphite, *J. Chem. Phys.* **21**, 1663 (1953).
- [19] G. A. Slack, Anisotropic thermal conductivity of pyrolytic graphite, *Phys. Rev.* **127**, 694 (1962).
- [20] R. Taylor, The thermal conductivity of pyrolytic graphite, *Philos. Mag.* **13**, 157 (1966).
- [21] T. Tanaka and H. Suzuki, The thermal diffusivity of pyrolytic graphite at high temperatures, *Carbon* **10**, 253 (1972).
- [22] J. P. Issi, J. Heremans, and M. S. Dresselhaus, Electronic and lattice contributions to the thermal conductivity of graphite intercalation compounds, *Phys. Rev. B* **27**, 1333 (1983).
- [23] J. Heremans, J. P. Issi, I. Zabala-Martinez, M. Shayegan, and M. S. Dresselhaus, Thermoelectric properties of a dilute graphite donor intercalation compound, *Phys. Lett. A* **84**, 387 (1981).
- [24] J. Boxus, B. Poulaert, J.-P. Issi, H. Mazurek, and M. S. Dresselhaus, Low temperature thermal conductivity of graphite-FeCl₃ intercalation compounds, *Solid State Commun.* **38**, 1117 (1981).
- [25] M. Dresselhaus and G. Dresselhaus, Intercalation compounds of graphite, *Adv. Phys.* **30**, 139 (1981).
- [26] C. Chiritescu, D. G. Cahill, C. Heideman, Q. Lin, C. Mortensen, N. T. Nguyen, D. Johnson, R. Rostek, and H. Böttner, Low thermal conductivity in nanoscale layered materials synthesized by the method of modulated elemental reactants, *J. Appl. Phys.* **104**, 033533 (2008).
- [27] W.-P. Hsieh, B. Chen, J. Li, P. Keblinski, and D. G. Cahill, Pressure tuning of the thermal conductivity of the layered muscovite crystal, *Phys. Rev. B* **80**, 180302 (2009).
- [28] P. G. Klemens and D. F. Pedraza, Thermal conductivity of graphite in the basal plane, *Carbon* **32**, 735 (1994).
- [29] Z. Chen, Z. Wei, Y. Chen, and C. Dames, Anisotropic debye model for the thermal boundary conductance, *Phys. Rev. B* **87**, 125426 (2013).
- [30] J. C. Duda, J. L. Smoyer, P. M. Norris, and P. E. Hopkins, Extension of the diffuse mismatch model for thermal boundary conductance between isotropic and anisotropic materials, *Appl. Phys. Lett.* **95**, 031912 (2009).
- [31] R. Prasher, Thermal boundary resistance and thermal conductivity of multiwalled carbon nanotubes, *Phys. Rev. B* **77**, 075424 (2008).
- [32] Z. Wei, Y. Chen, and C. Dames, Negative correlation between in-plane bonding strength and cross-plane thermal conductivity in a model layered material, *Appl. Phys. Lett.* **102**, 011901 (2013).
- [33] Z. Wei, J. Yang, W. Chen, K. Bi, D. Li, and Y. Chen, Phonon mean free path of graphite along the *c*-axis, *Appl. Phys. Lett.* **104**, 081903 (2014).
- [34] J. Yang, M. Shen, Y. Yang, W. J. Evans, Z. Wei, W. Chen, A. A. Zinn, Y. Chen, R. Prasher, T. T. Xu *et al.*, Phonon transport through point contacts between graphitic nanomaterials, *Phys. Rev. Lett.* **112**, 205901 (2014).
- [35] M. Harb, C. von Korff Schmising, H. Enquist, A. Jurgilaitis, I. Maximov, P. V. Shvets, A. N. Obratsov, D. Khakhulin, M. Wulff, and J. Larsson, The *c*-axis thermal conductivity of graphite film of nanometer thickness measured by time resolved x-ray diffraction, *Appl. Phys. Lett.* **101**, 233108 (2012).
- [36] G. Chen, *Nanoscale Energy Transport and Conversion* (Oxford University Press, New York, 2005).
- [37] C. Hua and A. J. Minnich, Transport regimes in quasiballistic heat conduction, *Phys. Rev. B* **89**, 094302 (2014).
- [38] B. Vermeersch, J. Carrete, N. Mingo, and A. Shakouri, Superdiffusive heat conduction in semiconductor alloys. I. Theoretical foundations, *Phys. Rev. B* **91**, 085202 (2015).
- [39] J. A. Johnson, A. A. Maznev, J. Cuffe, J. K. Eliason, A. J. Minnich, T. Kehoe, C. M. S. Torres, G. Chen, and K. A. Nelson, Direct measurement of room-temperature nondiffusive thermal transport over micron distances in a silicon membrane, *Phys. Rev. Lett.* **110**, 025901 (2013).
- [40] A. J. Minnich, M. S. Dresselhaus, Z. F. Ren, and G. Chen, Bulk nanostructured thermoelectric materials: Current research and future prospects, *Energy Environ. Sci.* **2**, 466 (2009) (Invited, peer-reviewed. Among the top 10 downloaded articles in EES for July, August, December 2009, January–May, July–December 2010, January 2011).
- [41] I. S. Gradshteyn and I. M. Ryzhik, *Table of Integrals, Series and Products* (Academic, New York, 1980).
- [42] J. Ma, W. Li, and X. Luo, Examining the callaway model for lattice thermal conductivity, *Phys. Rev. B* **90**, 035203 (2014).
- [43] A. J. Minnich, J. A. Johnson, A. J. Schmidt, K. Esfarjani, M. S. Dresselhaus, K. A. Nelson, and G. Chen, Thermal conductivity spectroscopy technique to measure phonon mean free paths, *Phys. Rev. Lett.* **107**, 095901 (2011).
- [44] A. J. Minnich, Determining phonon mean free paths from observations of quasiballistic thermal transport, *Phys. Rev. Lett.* **109**, 205901 (2012).
- [45] M. Grant and S. Boyd, in *Recent Advances in Learning and Control*, edited by V. Blondel, S. Boyd, and H. Kimura, Lecture Notes in Control and Information Sciences (Springer-Verlag Limited, Berlin, 2008), pp. 95–110.
- [46] M. Grant and S. Boyd, *CVX: Matlab Software for Disciplined Convex Programming, Version 1.21* (Springer-Verlag Limited, Berlin, 2011).